Accepted Manuscript

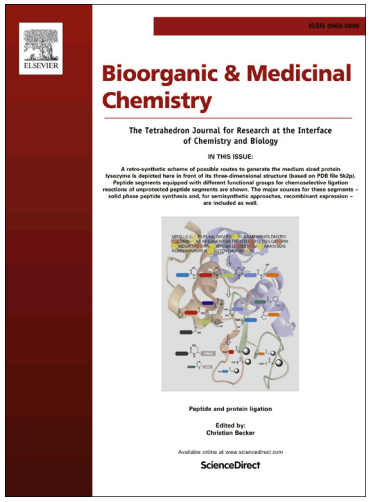

Synthesis and photophysical properties of a fluorescent cyanoquinoline probe for profiling ERBB2 kinase inhibitor response

Heajin Lee, Ralf Landgraf, James N. Wilson

PII: S0968-0896(17)30930-6
DOI: https://doi.org/10.1016/j.bmc.2017.09.034
Reference: BMC 13994

To appear in: *Bioorganic & Medicinal Chemistry*

Received Date: 20 July 2017
Revised Date: 21 September 2017
Accepted Date: 22 September 2017

Please cite this article as: Lee, H., Landgraf, R., Wilson, J.N., Synthesis and photophysical properties of a fluorescent cyanoquinoline probe for profiling ERBB2 kinase inhibitor response, *Bioorganic & Medicinal Chemistry* (2017), doi: https://doi.org/10.1016/j.bmc.2017.09.034

Graphical Abstract

Synthesis and photophysical properties of a fluorescent cyanoquinoline probe for profiling ERBB2 kinase inhibitor response

Leave this area blank for abstract info.

Heajin Lee, Ralf Landgraf, and James N. Wilson
Department of Chemistry, University of Miami, Coral Gables, Florida 33124, United States.
Department of Biochemistry and Molecular Biology, University of Miami, Miami, Florida 33101, United States.
Sylvester Comprehensive Cancer Center, University of Miami, Miami, Florida 33101, United States.

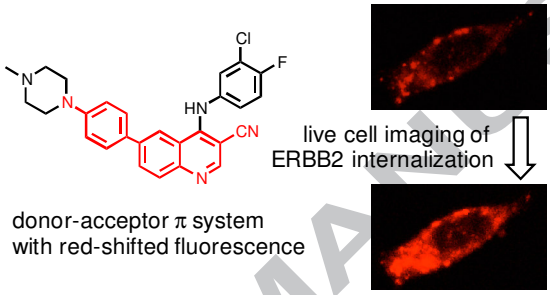

Bioorganic & Medicinal Chemistry
journal homepage: www.elsevier.com

Synthesis and photophysical properties of a fluorescent cyanoquinoline probe for profiling ERBB2 kinase inhibitor response

Heajin Lee,[a] Ralf Landgraf,[b,c]* and James N. Wilson[a,c]*

[a]*Department of Chemistry, University of Miami, Coral Gables, Florida 33124, United States.*
[b]*Department of Biochemistry and Molecular Biology, University of Miami, Miami, Florida 33101, United States.*
[c]*Sylvester Comprehensive Cancer Center, University of Miami, Miami, Florida 33101, United States.*

ARTICLE INFO

Article history:
Received
Received in revised form
Accepted
Available online

Keywords:
receptor tyrosine kinase
kinase inhibitor
fluorescent probe
EGFR
ERBB

ABSTRACT

A fluorescent probe targeting the ERBB2 receptor tyrosine was designed, synthesized and evaluated as reporter of ERBB2 dynamics in overexpressing BT474, i.e. Her2(+), cells. Two cyanoquinazoline (**CQ**) probes modeled after type-I (**CQ1**) or active state and type-II (**CQ2**) or inactive state inhibitors were designed and synthesized with extended π systems that impart binding-induced, turn-on fluorescence. Solution spectroscopy revealed that **CQ1** exhibited attractive photophysical properties and displayed turn-on emission in the presence of purified, soluble ERBB2 kinase domain, while **CQ2** was found to be non-emissive, likely due to quenching via a photoinduced electron transfer mechanism. Live cell imaging with **CQ1** revealed that this probe targeted an intracellular population of ERBB2, which increased following treatment with type-I inhibitors, gefinitib and canertinib, but showed no response to type-II inhibitors. **CQ1** thus provides a novel means of imaging the dynamic response of ERBB2(+) cells to kinase inhibitors.

1. Introduction

The advent of modern chemotherapies, including monoclonal antibodies and small molecule kinase inhibitors, has revolutionized the treatment of many cancers.[1] Yet, rapidly identifying the most effective treatment regime remains a challenge that is complicated by tumor heterogeneity, evolving mutations and compensatory shifts in signaling pathways that minimize the impact of targeted therapies.[2,3] Genomic analysis can provide great predictive power for the efficacy of certain drugs, but functional phenotypic assays are also a useful tool. To this end, we recently reported fluorescent kinase probes, kProbes, directed at the EGFR/ERBB family of receptor tyrosine kinases.[4-6] Modification of an N-phenyl quinazoline core, an established ERBB-targeted pharmacophore common to erlotinib, gefitinib and lapatinib,[7,8] introduced environmentally responsive fluorescence switching, such that the probes are non-emissive, or OFF in solution and become photoemissive upon binding, i.e. emission is switched ON.[4] This OFF/ON, or turn-on emission, response allows the membrane-permeable probes to be utilized on live cells, without the need for rinsing or removal of the unbound probe. First generation probes, **QA1** and **QA2** (Figure 1) were shown to selectively stain and differentiate ERBB2-overexpressing, i.e. Her2(+), cells, from low level expressing cells classified clinically as Her2(-).[6] While receptor activation dynamics could be reported in real time at the single cell level,[6] spectral overlap with the moderate inherent emission of small

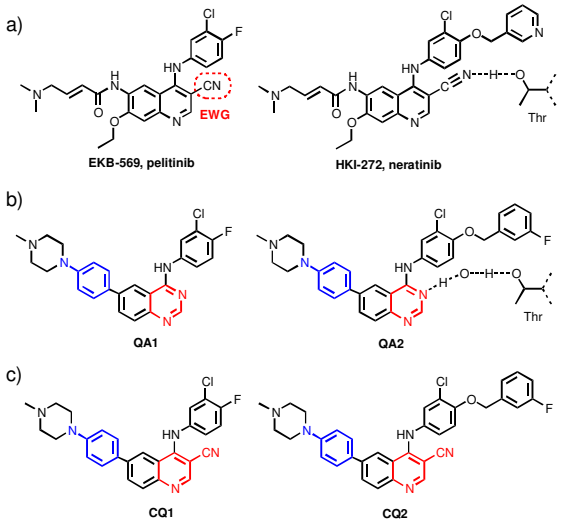

Figure 1. A) Examples of type-I, pelitinib, and type-II, neratinib, cyanoquinolines under investigation as EGFR/ERBB inhibitors; the cyano moiety interacts with a threonine residue in the ATP binding pocket, replacing a water bridge found for quinazoline inhibitors.[12,13] B) Fluorescent quinazoline probes developed in our lab. C) Cyanoquinoline probes with modified donor-π-acceptor investigated in this study.

molecule inhibitors,[9] such as lapatinib[10] or gefitinib,[11] prevented the use of **QA1** and **QA2** for assaying the effect of these drugs. To maximize the utility of these fluorescent reporters in novel drug screens or mechanistic dissection of signaling pathways using established inhibitors, the optical properties of fluorescent kProbes needs to be tuned to minimize spectral overlap with typically UV to blue emissive pharmacophores.

In this contribution, we report the design, synthesis and optical properties of cyanoquinoline kProbes, which exhibit significantly red-shifted fluorescence compared to their quinazoline predecessors. The optical properties of **CQ1**, in particular, make it an attractive candidate for both detecting ERBB2-expressing cells, as well as monitoring drug response. **CQ1** exhibits a large Stokes shift, with emission centered at 520 nm, and a high turn-on, i.e. ON/OFF, ratio between the ERBB-bound/unbound forms. With these improved photophysical parameters, **CQ1** is optically compatible with many ERBB2-targeted kinase inhibitors, and can be utilized to explore cellular responses to drug exposure. **CQ1** stains the intracellular pool of ERBB2, which is not typically accessible to antibody labeling in a live cell setting. Finally, we demonstrate the use of **CQ1** to image the dynamics of Gefitinib-induced internalization of ERBB2.

2. Results and Discussion

2.1. Design and Synthesis

Several quinazoline-based inhibitors, such as erlotinib, gefitinib and lapatinib, target the ATP binding fold of the EGFR/ERBB family.[7,8] In some cases, the inherent fluorescence of these inhibitors allows for tracking of their subcellular distribution,[10,11] yet their properties as fluorescent probes are less than ideal, requiring UV excitation and exhibiting low quantum yields. However, at clinically relevant concentrations (1-10 μM) they are sufficiently emissive to contribute to moderate background emission that overlaps with our recently reported ERBB2-targeted kProbes, **QA1** and **QA2**. Thus, we set out to develop next generation probes with significantly red shifted emission spectra required to image the dynamics of this receptor tyrosine kinase family in response to these quinazoline-based inhibitors. 3-Cyanoquinolines, including pelitinib and neratinib,[12,13] have also been demonstrated as inhibitors of these receptor tyrosine kinases. Their binding mode differs slightly with the cyano group replacing a bridging water molecule, which interacts with a threonine residue via a hydrogen bond as shown in Figure 1 with neratinib versus **QA2**. Our investigations into the optical properties of several donor-acceptor quinazoline π-systems demonstrated that strong electron-withdrawing groups effectively lowered the energy of the S_1 state producing a concomitant red shift in both the absorption and excitation spectra of model quinazoline kProbes.[5]

Based on quantum chemical calculations, we anticipated that switching from the moderately electron-withdrawing nitrogen atom at the 3-position of **QA1** or **QA2** to the stronger electron withdrawing nitrile group of the cyanoquinoline probes, **CQ1** and **CQ2**, could generate a probe with red-shifted excitation and emission spectra. DFT calculations on truncated model compounds **QA** and **CQ** (Figure 2) predicted an S_1 state that was only lowered by 0.3 eV, corresponding to a ~25 nm shift in the absorption spectra. However, mapping of the frontier molecular orbitals, as well as the dipoles of the molecules, 6.6 D for **QA** versus 8.9 D for **CQ**, suggested that the excited state of the cyanoquinoline probes should be more polarized than that of of the quinazoline probes. This can be seen in a small, but non-trivial shift in orbital density in the frontier molecular orbitals. While the HOMOs of **QA** and **CQ** are virtually identical, the

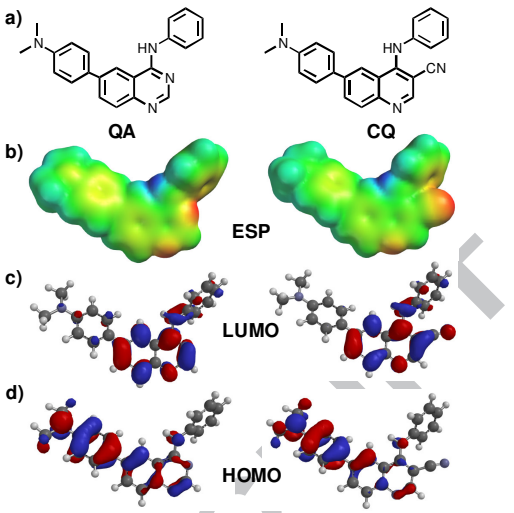

Figure 2. a) Chemical structures, b) electrostatic potential map and c, d) frontier molecular orbitals of model compounds used to compare the electronic properties of kinase probes buiilt on the quinazoline (**QA**) and cyanoquinoline (**CQ**) heterocyclic cores. While the HOMOs map with nearly identical distributions, the LUMO shows slightly more polarization on **CQ**, a result of the electron-withdrawing nature of the cyano group, which also appears electronegative in the ESP surface.

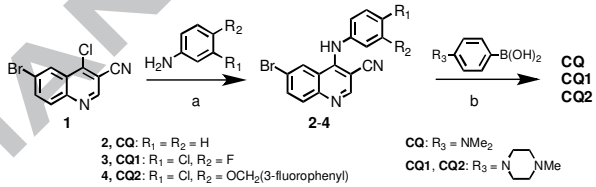

Figure 3. Synthesis of fluorescent cyanoquinoline probes. Conditions: a) 2-propanol, 80° C, 24 h; b) $Pd(OAc)_2$, PPh_3, Et_3N, DMF, 80° C, 24 h.

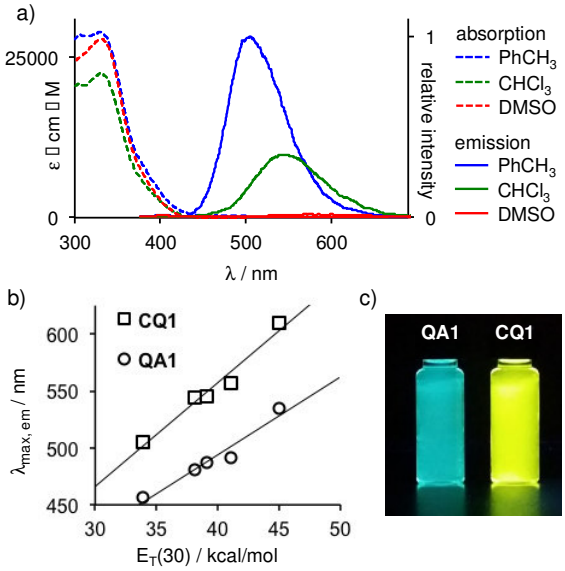

Figure 4. a) Absorption and emission spectra of **CQ1** in several solvents demonstrating the sensitivity of the excited state to solvent polarity. b) Comparison of the emission maxima of **CQ1** and **QA1** in various solvents reveals that the cyanoquinoline core of **CQ1** is slightly more responsive to solvent polarity. c) A visual comparison of **QA1** and **CQ1** in chloroform shows the red-shifted emission of **CQ1**.

LUMO of **CQ** showed density shifted away from the dimethylamino group and towards the cyano group, which could contribute to thermal relaxation in the excited state and an increased Stokes shift.

The synthesis (Figure 3) of **CQ1** and **CQ2** proceeded from 6-bromo-4-chloro-3-quinolinecarbonitrile (**1**) which was generated according to reference 14 and confirmed by ^{1}H and ^{13}C NMR spectroscopy (see Supplementary Material) as well as HRMS. The two pharmacophore arms, or phenyl moiety in the case of the model compound, **CQ**, were installed via nucleophilic aromatic substitution of the chlorine at the 4-position, followed by the electron-donating anilino arm, which coupled under Suzuki conditions to the 6-position. The compounds were obtained as bright yellow solids following column chromatography and crystallization. Ki values of 390 nM and 590 nM were determined for **CQ1** and **CQ2**, respectively, in receptor stimulation assays (see Experimental section, below).

2.2. Optical Properties

We first examined the optical properties of **CQ1** and **CQ2** in organic solvents to evaluate their sensitivity to their chemical environment and polarity-dependent fluorescence (Figure 4). Additionally, moderately polar organic solvents, such as $CHCl_3$, closely match the apparent polarity of the ATP binding pocket of ERBB2 and emission in these solvents informs our imaging parameters for fluorescence microscopy.[5] UV-vis absorption spectroscopy showed little variation between solvents, with peak absorption at 330 nm and ε varying slightly from 2.5 x 10^4 cm^{-1} $M^{-1}$to 2.9 x 10^4 cm^{-1} M^{-1} for both compounds, however, fluorescence spectroscopy showed marked differences. **CQ1** was emissive in solvents of low polarity, such as toluene (Φ_{em} = 0.38) with an E_T30 value of 33.9 kcal/mol on Reichardt's scale, and chloroform (Φ_{em} = 0.21) with an E_T30 value of 39.1 kcal/mol, but essentially nonemissive in solvents more polar that DMSO (E_T30 = 45.0 kcal/mol).[15] Emission was completely quenched in water, octanol, methanol and acetonitrile, which have ET30 values ranging from 46.0 to 63.1 kcal/mol. A linear correlation between solvent polarity and emission wavelength was found by examining several other solvents (Figure 4b) and the shift in emission wavelength was found to be higher for **CQ1** compared to **QA1**, demonstrating that the more polar excited state was better stabilized in polar solvents. The marked red-shift in the emission spectra of **CQ1**, relative to **QA1**, is also apparent by eye when comparing the probes in identical solvents, as shown in Figure 4c. This again is testament to the presencet of the electron-withdrawing nitrile, which lowers the energy of the S_1 state. While **CQ1** was found to be emissive, **CQ2** showed no emission in any solvent. By comparison, the quinazoline analog, **QA2**, was weakly emissive in relation to **QA1**. The addition of the type 2 pharmacophore arm appears to have a quenching effect on both the 3-cyanoquinoline and quinazoline fluorophore cores, which is exacerbated by the presence of the electron withdrawing cyano group. We attribute this quenching to an excited state electron transfer process, from the electron-rich N-phenyl-benzyloxy ether.[16] Thus, while **CQ2** is cannot be utilized as a fluorescent turn-on probe, **CQ1** is ideally suited as a red-emissive, type 1 inhibitor.

We next investigated the binding-induced, turn-on emission of **CQ1** and its optical compatibility with several commercially available inhibitors in the presence of purified ERBB2 kinase domain. As shown in Figure 5, the excitation spectra of ERBB2-bound **CQ1** is similar to ERBB2-bound **QA1** and overlaps significantly with quinazoline-based ERBB inhibitors such as gefitinib and lapatinib. However, **CQ1** is distinguishable from **QA1**, gefitnib and lapatinib through a large, 200 nm Stokes shift,

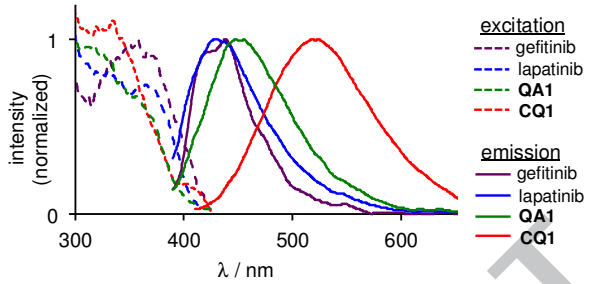

Figure 5. Comparison of excitation and emission spectra, in the presence of purified ERBB2 kinase domain, of two quinazoline inhibitors, gefitinib and lapatinib, with quinazoline probe, **QA1** and cyanoquinoline probe, **CQ1**. While all four compounds share similar excitation spectra, the emission of **CQ1** is significantly red-shifted, allowing for selective imaging of ERBB2-binding in cells treated with ERBB2-targeted inhibitors. Inset shows a comparison of **QA1** and **CQ1** emission in $CHCl_3$.

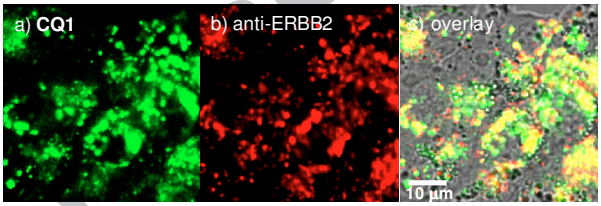

Figure 6. CQ1 colocalizes with anti-ERBB2 staining: a) the false-colored green channel shows **CQ1** distribution, λ_{ex} = 405 nm, λ_{em} = 500 - 600 nm; b) the false-colored red channel shows antibody staining of ERBB2; c) overlay of the two channels shows a high degree of overlap.

which sufficiently segregates the emission of this probe from the kinase inhibitors. The emission maximum of the bound form of **CQ1** is 520 nm, compared to 440 nm for ERBB2-bound lapatinib and gefitinib, providing a unique optical window that allows for selective monitoring of **CQ1** emission in the presence of ERBB2-directed inhibitors. Having established the optical compatibility of CQ1 with quinazoline-based inhibitors, we next examined the live cell imaging capabilities of this probe.

2.3. Confocal Microscopy

We next evaluated **CQ1** as an ERBB2-targeted probe in a live cell setting using BT474 cells, which are classified clinically as Her2(+) and express ~10^6 copies of ERBB2. Cells were first stained with ERBB2-directed antibody, then treated with 2 µM solutions of **CQ1**. Figure 6 shows the two-channel image of the **CQ1** (green) and anti-ERBB2 (red) staining, which show a high degree of overlap in the merged image. Minimal cell surface staining was observed for **CQ1**, indicative of binding to internalized receptors, and longer antibody staining times (12-16 h) were required to access this internalized pool of ERBB2. By contrast, the small molecule, membrane-permeable probe required only 5 min of staining to saturate the same population.

Having established that **CQ1** targets ERBB2 in live cells, our final goal was to demonstrate the compatibility of probe with clinically-relevant inhibitors. Gefitinib provides an interesting case-study for ERBB2 dynamics as it is a low-affinity inhibitor of ERBB2, with IC50 values varying widely from 0.24 µM[17] to in excess of 5 µM[18-20] and linked to factors such as expression level,[21,22] tumor type[18] and binding pocket mutations.[20,23] In terms of receptor dynamics, Gefitinib has been shown to induce heterodimerization[24] and internalization of ERBB2[25] providing an excellent opportunity to track dynamic ERBB2 pools with **CQ1** as a fluorescent reporter. This is evident in the time-dependent

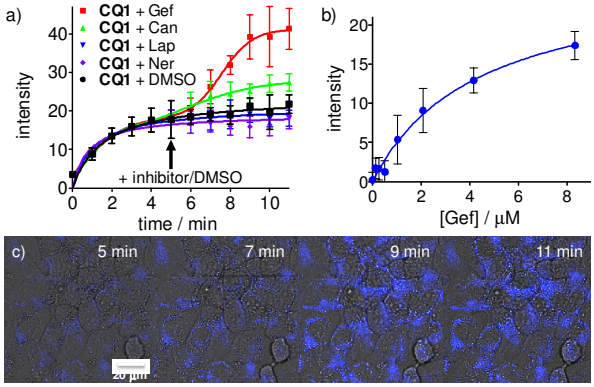

Figure 7. Imaging of geftinib-induced, active conformation ERBB2-internalization: a) following CQ1 saturation of ERBB2, the addition of gefitinib, and to a lesser extent canertinib, both active conformer inhibitors, produces an increase in **CQ1** emission intensity, while the addition of inactive state inhibitors, lapatinib or neratinib, does not; b) the gefitinib-induced emission increase shows a concentration dependence, with and EC50 of 4.4 µM that closes matches the reported IC50 values of 3.7 to 3.9 µM;[18,19] c) images of time dependent increase in emission in BT474 cells;

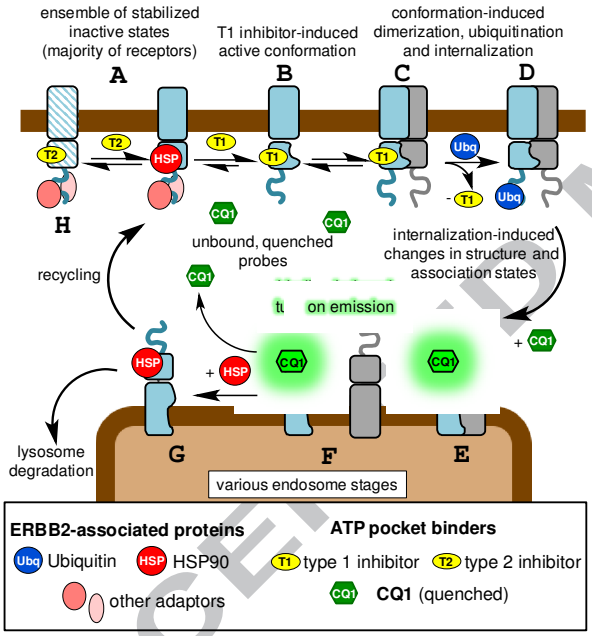

Figure 8. Stages in ERBB receptor signaling and model for potential interplay of **CQ1** and inhibitor binding: The active and inactive kinase conformations on the cell surface (A-D) preferentially associate with, and are stabilized by, distinct interaction partners. Binding of type-I and type-II inhibitors (**T1**, **T2**) shifts the equilibrium of association states and is known to drive both dimerization and internalization.[24-29] Internalization results in a change in association states and pH-induced changes in interactions and conformations of the extracellular domains (E-G).[30-32] At present, little is known about the relative affinity of established inhibitors and competition with kinase directed probes in these distinct states. Current data on probe **CQ1** (shown in on- and off-state) suggest that probe binding is favored in the internalized state.

emission intensity of cells first treated with **CQ1**, followed by gefitinib treatment (red trace, Figure 7a). BT474 cells were exposed to 2 µM solutions of **CQ1** and after 5 min, the signal had plateaued, indicating saturation of the internal ERBB2 population. Subsequent addition of gefitinib (5 µM), induced a second wave of emission increase, which stabilized after 5-6 min. The gefitinib-induced response was found to be concentration dependent, as shown in Figure 7b, with an EC50 of 4.4 µM. This value correlates very well with the average IC50 value of 3.9 µM reported across several tumor types.[18] While gefitnib and **CQ1** target the same binding fold, **CQ1**, with a Ki of 390 nM and used at 2 µM can effectively compete with gefitinib to access the binding pocket and report ERBB2 internalization. To verify this behavior, we also evaluated the effect of canertinib and compared it to two type-II, i.e. inactive state inhibitors, lapatinib and neratinib (blue and purple traces, Figure 7a). Canertinib (green trace, Figure 7a) induces a more moderate increase in **CQ1** emission that can be rationalized on the basis of higher affinity and ability to bind covalently, blocking competition from **CQ1**.[26] By contrast, neither inactive state inhibitor elicited an increase in **CQ1**, supporting the notion and structural features that **CQ1** binding is to the active state.[27] The possible interactions for ERBB2 with type-I and type-II probes, as well as CQ1, are summarized Figure 8.[27-29] **CQ1** thus provides a route not only to image the internal pool of ERBB2 and dynamics of internalization, but also to differentiate drug binding modes which is linked to their effects on receptor conformation, dimerization and internalization.

3. Conclusions

In summary, we have developed an ERBB2-targeted kinase probe, **CQ1**, utilizing a 3-cyanoquinoline core, studied the optical as well as biochemical properties, and demonstrated its utility in imaging dynamic shifts in receptor populations in response to various ERBB2-targeted inhibitors. The optical properties of **CQ1** were improved over previous fluorescent reporters, owing to the presence of the nitrile group serves to stabilize the charge transfer excited state and red-shift emission of the probe beyond that observed for early generation probes and clinically relevant EGFR/ERBB inhibitors. **CQ1** was found to have moderate affinity for ERBB2 and targets the intracellular pool, allowing this probe to function as a reporter of the rapid dynamics of kinase internalization, following inhibitor treatment. Finally, we were able to differentiate the response of inhibitors targeting the active and inactive conformation. These results serve as a demonstration of the utility of a small molecule fluorescent reporter that is membrane permeable and can target an intracellular binding pocket. Future development of kinase-specific probes, adapted from existing and clinically available inhibitors, can complement established antibody-labeling strategies, providing information about dynamic shifts in kinase populations in response to specific drug treatments.

4. Experimental section

4.1. Chemistry

4.1.1. Synthesis of 6-bromo-N-(phenyl)-quinoline-3-carbnitrile-4-amine (2).

2.5 grams of **1** (9.4 mmol), 1.5 g (16.1 mmol) of aniline, and 2-propanol were added, vigorously stirred and heated at 80 °C, overnight with a condenser. After 24 hours, it was cooled to room temperature, concentrated under reduced pressure, 100 mL of 1M KOH solution was added and stirred for 20 min, 300 mL of EtOAc was added, then organic solution was extracted through separation funnel and concentrated. It was purified over silica (100% DCM to 100% EtOAc) followed by crystallization from methanol to afford yellow powder of **2** (1.363g, 42.1 %); mp: 216-218℃ ; IR ν_{max}(cm^{-1}): 3279.7, 3202.7, 3123.3, 3053.9, 2226.2, 1865.0, 1739.3, 1608.8, 1582.8, 1557.1, 1495.6, 1447.6, 1353.1, 1318.5, 1274.8, 1232.3, 1117.0, 1077.7, 971.2, 826.9,

769.3, 696.5, 610.5; ^{1}H NMR(500 MHz, DMSO-d_6), δ: 7.26-7.32 (m, 3H), 7.41 (t, 2H, J = 8.0 Hz), 7.86 (d, 1H, J = 8.5 Hz), 7.97 (dd, 1H, J = 8.5, 1.5 Hz), 8.60 (s, 1H), 8.78 (s, 1H), 9.92 (s, 1H); ^{13}C NMR (125 MHz, DMSO-d_6), δ: 88.82, 116.91, 120.01, 121.16, 125.00, 125.86, 126.54, 129.50, 132.03, 135.30, 139.48, 147.88, 150.69, 154.02; HR-ESI (Q-TOF) m/z: calculated for $C_{16}H_{11}BrN_3^+$ (M+H$^+$): 324.0136, found: 324.0135.

*4.1.2. Synthesis of 6-bromo-N-(3-chloro-4-fluoro-phenyl)-quinoline-3-carbnitrile-4-amine (**3**).*

1.0 grams of **1** (3.8 mmol), 0.8 g (5.5 mmol) of 3-chloro-4-fluoro-aniline, and 2-propanol were added, vigorously stirred and heated at 80 ^{o}C, overnight with a condenser. After 24 hours, it was cooled to room temperature, concentrated under reduced pressure, 50 mL of 1M KOH solution was added and stirred for 20 min, 100 mL of EtOAc was added, then organic solution was extracted three times through separation funnel and concentrated. It was crystallization from methanol, ethyl acetate to afford yellow powder of **3** (553 mg, 38.8 %); mp: 210-212℃ ; IR ν_{max}(cm^{-1}): 3528.2, 3328.5, 3223.7, 3178.0, 3090.5, 3038.5, 2917.7, 2849.4, 2214.1, 1900.6, 1733.8, 1607.0, 1581.6, 1560.0, 1486.9, 1415.3, 1353.2, 1257.2, 1220.2, 1117.6, 1075.0, 978.2, 821.5, 771.3, 673.2, 650.9; ^{1}H NMR(500 MHz, DMSO-d_6), δ: 7.37 (s, 1H), 7.46 (t, 1H, J = 8.5 Hz), 7.62 (s, 1H), 7.89 (s, 1H), 7.98 (d, 1H, J = 8.0 Hz), 8.63 (s, 1H), 8.74 (s, 1H), 9.97 (s, 1H); ^{13}C NMR (125 MHz, DMSO-d_6), δ: 88.60, 117.01, 117.49-117.66 (d, $J_{C,F}$ = 21.25 Hz), 120.05-120.10 (d, $J_{C,F}$= 6.25 Hz), 120.20, 121.11, 125.81, 126.04-126.08 (d, $J_{C,F}$ = 5.0 Hz), 127.27, 131.76, 135.38, 137.06, 147.52, 150.77, 153.71, 154.83-156.78 (d, $J_{C,F}$ = 243.75 Hz); HR-ESI (Q-TOF) m/z: calculated for $C_{16}H_8BrClFN_3^+$ (M+H$^+$): 377.9632, found: 377.9632.

*4.1.3. Synthesis of 6-bromo-N-(3-chloro-4-((3-fluorophenyl)methoxy)phenyl)-quinoline-3-carbnitrile-4-amine (**4**).*

1.0 grams of **1** (3.8 mmol), 1.38 g (5.5 mmol) of 3-chloro-4-[(3-fluorophenyl)methoxy]-benzenamine, and 2-propanol were added, vigorously stirred and heated at 80 ^{o}C, overnight with a condenser. After 24 hours, it was cooled to room temperature, concentrated under reduced pressure, 50 mL of 1M KOH solution was added and stirred for 20 min, 100 mL of EtOAc was added, then organic solution was extracted three times through separation funnel and concentrated. It was crystallization from methanol, ethyl acetate to afford yellow powder of **4** (647 mg, 35.4 %); mp: 208-210℃ ; IR ν_{max}(cm^{-1}):3366.4, 3074.0, 2923.7, 2205.9, 1870.6, 1739.3, 1606.5, 1582.9, 1559.9, 1500.7, 1447.1, 1353.5, 1311.4, 1288.5, 1268.8, 1221.9, 1117.7, 1059.4, 1027.2, 979.4, 894.3, 805.7, 745.8, 682.6, 610.5; ^{1}H NMR(500 MHz, DMSO-d_6), δ: 5.28 (s, 2H), 7.17 (t, 1H, J = 8.0 Hz), 7.26-7.34 (m, 4H), 7.45-7.50 (m, 2H), 7.85 (d, 1H, J = 9.0 Hz), 7.97 (d, 1H, J = 7.5 Hz), 8.57 (s, 1H), 8.76 (s, 1H), 9.87 (s, 1H); ^{13}C NMR (125 MHz, DMSO-d_6), δ: 69.86, 87.72, 114.42-114.60 (d, $J_{C,F}$= 22.5 Hz), 114.75, 115.10-115.27 (d, $J_{C,F}$= 21.25 Hz), 117.09, 119.94, 120.71, 122.09, 123.79-123.81 (d, $J_{C,F}$= 2.5 Hz), 125.70, 126.22, 127.89, 130.98-131.04 (d, $J_{C,F}$= 7.5 Hz), 132.01, 132.99, 135.27, 139.82-139.88 (d, $J_{C,F}$= 7.5 Hz), 147.72, 151.12, 152.47, 154.09, 161.69-163.63 (d, $J_{C,F}$= 242.5 Hz); HR-ESI (Q-TOF) m/z: calculated for $C_{23}H_{15}BrClFN_3O^+$ (M+H$^+$): 484.0051, found: 484.0051.

*4.1.4. Synthesis of 6-(4-(Dimethyl-amino)phenyl)-N-(phenyl)-quinoline-3-carbonitrile-4-amine (**CQ**).*

0.8 g (2.5 mmol) of 6-bromo-N-(phenyl)-quinoline-3-carbnitrile-4-amine, 650 mg (3.2 mmol) of 4-(dimethylamino)phenylboronic acid hydrochloride, 80 mg of PPh_3, 10 mL of Et_3N, and 10 mL of DMF were placed in a 50 mL Schlenk flask with a stirrer bar under nitrogen purge. The reaction mixture was degassed for a further 30 min under a slow stream of nitrogen, at which point 80 mg of $Pd(OAc)_2$ was added. The reaction mixture was heated at 80 ^{o}C for 24 h, cooled, filtered through filter paper and eluted solution was added into 50 mL of H_2O directly, and ethyl acetate was poured onto funnel to wash the residues. Water and ethyl acetate solution mixture went through extraction with three times with 200 mL of ethyl acetate each. The organic layer was dried with $MgSO_4$, filtered, and then concentrated under reduced pressure. The solid was crystalized in methanol, ethylacetate multiple times to afford light yellow powder of **CQ**. (165.0 mg, 18.1 %); mp: 275-276℃ (dec); IR ν_{max}(cm^{-1}): 3197.2, 3159.9, 3082.3, 3060.4, 2989.3, 2888.7, 2814.2, 2220.7, 1944.4, 1851.4, 1733.8, 1603.5, 1577.8, 1547.0, 1494.6, 1445.7, 1363.5, 1308.5, 1297.3, 1263.6, 1063.1, 965.9, 898.4, 808.6, 762.3, 691.6, 622.3; ^{1}H NMR(500 MHz, DMSO-d_6), δ: 2.97 (s, 6H), 6.84 (d, 2H, J = 9.0 Hz), 7.25 (t, 1H, , J = 7.5 Hz), 7.32 (d, 2H, J = 8.0 Hz), 7.42 (t, 2H, J = 7.5 Hz), 7.75 (d, 2H, J = 9.0 Hz), 7.93 (d, 1H, J = 9.0 Hz), 8.13 (dd, 1H, J = 9.0, 1.5 Hz), 8.51 (s, 1H), 8.67 (d, 1H, J = 1.5 Hz), 9.90(s, 1H); ^{13}C NMR (125 MHz, DMSO-d_6), δ: 40.44, 88.51, 112.96, 117.44, 118.50, 120.09, 124.99, 126.26, 126.48, 128.09, 129.52, 130.33, 130.46, 138.79, 140.04, 147.76, 150.68, 151.38, 152.49; HR-ESI (Q-TOF) m/z: calculated for $C_{24}H_{21}N_4^+$ (M+H$^+$): 365.1766, found:365.1763.

*4.1.5. 6-(4-(4-Methylpiperazin-1-yl)phenyl)-N-(3-chloro-4-fluoro-phenyl)-quinoline-3-carbonitrile-4-amine (**CQ1**).*

500 milligrams (1.3 mmol) of 6-bromo-N-(3-chloro-4-fluoro-phenyl)-quinoline-3-carbnitrile-4-amine, 450 mg (2.0 mmol) of 4-(4-Methylpiperazin-1-yl)phenylboronic acid , 50 mg of PPh_3, 10 mL of Et_3N, and 10 mL of DMF were placed in a 50 mL Schlenk flask with a stirrer bar under nitrogen purge. The reaction mixture was degassed for a further 30 min under a slow stream of nitrogen, at which point 50 mg of $Pd(OAc)_2$ was added. The reaction mixture was heated at 80 ^{o}C for 24 h, cooled, filtered through filter paper and eluted solution was added into 50 mL of H_2O directly, and ethyl acetate was poured onto funnel to wash the residues. Water and ethyl acetate solution mixture went through extraction with three times with 200 mL of ethyl acetate each. The organic layer was dried with $MgSO_4$, filtered, and then concentrated under reduced pressure. It was purified over silica (100 % EtOAc to 100% MeOH), followed by crystallization in methanol, ethyl acetate multiple times to afford light yellow powder of **CQ1** (145.2 mg, 23.7 %); mp: 220-222℃ (dec); IR ν_{max}(cm^{-1}): 3571.1, 3331.2, 3170.1, 2965.5, 2937.8, 2888.0, 2836.3, 2811.5, 2211.6, 1867.8, 1766.6, 1663.0, 1602.4, 1587.4, 1533.9, 1494.3, 1414.9, 1361.1, 1254.5, 1128.5, 1077.6, 1009.2, 973.1, 844.4, 773.8, 655.2; ^{1}H NMR(500 MHz, DMSO-d_6), δ: 2.22 (s, 3H), 2.46 (broad s, 4H), 3.22 (broad s, 4H), 7.05 (d, 2H, J = 7.5 Hz), 7.38 (s, 1H), 7.47 (t, 1H, , J = 9.0 Hz), 7.61 (s, 1H), 7.76 (d, 2H, J = 7.5 Hz), 7.93 (d, 1H, J = 8.5 Hz), 8.13 (d, 1H, J = 8.0 Hz), 8.55 (s, 1H), 8.67 (s, 1H), 10.00 (s, 1H); ^{13}C NMR (125 MHz, DMSO-d_6 + TFA), δ: 42.56, 45.65, 52.59, 88.10, 116.50, 117.15, 117.55-117.72 (d, $J_{C,F}$= 21.25 Hz), 119.38, 119.85, 120.10-120.25 (d, $J_{C,F}$= 18.75 Hz), 126.36-126.42 (d, $J_{C,F}$= 7.5 Hz), 127.62, 128.26, 129.41, 130.17, 131.08, 137.15, 138.48, 146.65, 149.87, 152.02, 152.34, 154.94-156.89 (d, $J_{C,F}$= 243.75 Hz); HR-ESI (Q-TOF) m/z: calculated for $C_{27}H_{24}ClFN_5^+$ (M+H$^+$): 472.1704, found: 472.1673.

*4.1.6. 6-(4-(4-Methylpiperazin-1-yl)phenyl)-N-(3-chloro-4-((3-fluorophenyl)methoxy)phenyl)-quinoline-3-carbonitrile-4-amine (**CQ2**).*

500 milligrams (1.0 mmol) of **4**, 450 mg (2.0 mmol) of 4-(4-Methylpiperazin-1-yl)phenylboronic acid, 50 mg of PPh_3, 10 mL of Et_3N, and 10 mL of DMF were placed in a 50 mL Schlenk

flask with a stirrer bar under nitrogen purge. The reaction mixture was degassed for a further 30 min under a slow stream of nitrogen, at which point 50 mg of $Pd(OAc)_2$ was added. The reaction mixture was heated at 80 °C for 24 h, cooled, filtered through filter paper and eluted solution was added into 50 mL of H_2O directly, and ethyl acetate was poured onto funnel to wash the residues. Water and ethyl acetate solution mixture went through extraction with three times with 200 mL of ethyl acetate each. The organic layer was dried with $MgSO_4$, filtered, and then concentrated under reduced pressure. It was purified over silica (100 % EtOAc to 100% MeOH), followed by crystallization from methanol, ethyl acetate multiple times to afford yellow powder of **CQ2** (74.0 mg, 12.8 %); mp: 254-256℃ (dec); IR $\nu_{max}(cm^{-1})$: 3353.9, 3071.4, 2970.2, 2937.4, 2847.0, 2804.1, 2199.9, 1870.6, 1605.7, 1583.1, 1514.2, 1443.3, 1359.9, 1299.3, 1264.8, 1215.1, 1161.9, 1060.5, 1030.4, 1009.4, 953.2, 889.5, 784.5, 748.6, 690.0, 657.3; ^{1}H NMR(500 MHz, DMSO-d_6), δ: 2.23 (s, 3H), 2.47 (broad s, 4H), 3.23 (broad s, 4H), 5.29 (s, 2H), 7.06 (d, 2H, J = 9.0 Hz), 7.17 (t, 1H, , J = 8.0 Hz), 7.28-7.35 (m, 4H), 7.45 (q, 1H, J = 8.0 Hz), 7.52 (s, 1H), 7.77 (d, 2H, J = 9.0 Hz), 7.92 (d, 1H, J = 8.5 Hz), 8.14 (d, 1H, J = 7.5 Hz), 8.50 (s, 1H), 8.69 (s, 1H), 9.88 (s, 1H); ^{13}C NMR (125 MHz, DMSO-d_6), δ: 46.26, 48.07, 54.97, 69.86, 87.26, 114.42-114.60 (d, $J_{C,F}$= 22.5 Hz), 114.80, 115.10-115.27 (d, $J_{C,F}$= 21.25 Hz), 115.76, 117.57, 118.82, 119.56, 122.11, 123.79-123-81 (d, $J_{C,F}$= 2.5 Hz), 126.24, 127.94, 128.04, 129.01, 130.33, 130.50, 130.98-131.05 (d, $J_{C,F}$= 8.75 Hz), 133.49, 138.39, 139.85-139.91 (d, $J_{C,F}$= 7.5 Hz), 147.74, 151.25, 151.85, 152.32, 152.82, 161.70-163.64 (d, $J_{C,F}$= 242.5 Hz); HR-ESI (Q-TOF) m/z: calculated for $C_{34}H_{30}ClFN_5O^+$ ($M+H^+$): 578.2123, found: 578.2117.

4.2. Biological assays and imaging

4.2.1. Cell culture and reagents

MCF7 and BT474 cells were cultured as previously described[6] in sterile T-35 or T-75 flasks. Cells were maintained in RPMI containing 10% dialyzed FBS, penicillin (100 units/mL) and streptomycin (0.01%) solution under a humidified 5% CO_2 atmosphere.

4.2.2. Ligand stimulation assays

MCF7 cells were seeded with equal quantity (200 thousand/well) in six-well plates. After 48 hours, cells were pre-treated with the small molecule inhibitors of various concentrations for 1 hour before induction by neuregulin (NRGb1, 30 nM, 30 minutes). Cell lysates were generated immediately by SDS lysis. Equal aliquots were subjected to SDS-PAGE and Western blot analysis. ERBB2 phosphorylation was evaluated for Tyr1139 located close to the extreme cytoplasmic C-terminus of the receptor (validated by pan-TyrP detection (4G10)). The signal obtained for pTyr1139 relative to the ERBB2 receptor levels was determined as the relative receptor phosphorylation.

4.2.3. Confocal imaging

For imaging, cells were seeded at a density of 10^5 cell/cm^2 in 96 microwell plates or on glass coverslips. Cells maintained a normal morphology during the course of the experiments (maximum of 1 h) and remained adhered to the imaging plate or coverslip. Single photon imaging was performed on a Leica SP5 confocal microscope housed within the UM Biology Imaging Core Facility. For the imaging of **CQ1** a channel was created with excitation via a 405 nm laser line with emission between 500 and 600 nm captured and false-colored blue. Cells were labeled an anti-ERBB2 antibody directed towards the extracellular domain of ERBB2 followed by either Alexafluor 488 or 546 secondary antibody. Alexfluor 488 was imaged in a false-colored green channel with the following parameters: excitation was via the 488 nm laser line and emission was captured between 500 and 550 nm. Alexfluor 546 was imaged in a false-colored red channel with the following parameters: excitation was via the 561 nm laser line and emission was captured between 575 and 600 nm. Images were processed in Fiji.[33]

For time course measurements, the focal plane was first established using the phase contrast image and checked against the autofluorescence of the cells under illumination from the 405 nm laser line. Laser intensity and photodetector gain were set by imaging BT474 cells pretreated with either **CQ1** (2 μM, 10 minutes). All data time course data was collected on the same day with the same imaging settings. If z-drift was observed during the course of a timed experiment, the experiment was halted, the sample brought quickly (< 10 sec) into focus and the experiment was resumed. If z-drift persisted or longer refocusing times were required, the experiment was aborted and data collection began anew on a separate sample.

4.3. Quantum Chemical Calculations

Quantum chemical calculations were performed in Spartan. The structures of **QA** and **CQ** were optimized in the ground state (DFT 6-31G*) with the N-phenyl ring locked with dihedral angles matching the crystal structure of the ERBB1-bound inhibitor, gefitinib (PDB entry: 4WKQ).

Acknowledgments

This work was supported by the National Cancer Institute Innovative Molecular Analysis Technologies Program, CA182341-03 (J. N. W. and R. L.). J. N. W. also acknowledges seed funding from the American Cancer Society (98-277-07) R.L. also acknowledges the support of National Cancer Institute, CA98881-05 and the Braman Family Breast Cancer Institute.

References and notes

1. Chabner, B. A.; Roberts, T. G. *Nat. Rev. Cancer* **2005**, *5*, 65-72.
2. Bagnyukova, T.; Serebriiskii, I. G.; Zhou, Y.; Hopper-Borge, E. A.; Golemis, E. A.; Astsaturov, I. *Cancer Biol. Ther.* **2010**, *10*, 839-853.
3. McGranahan, N.; Swanton, C. *Cancer Cell* **2015**, *27*, 15-26.
4. Sicard, R.; Dhuguru, J.; Liu, W.; Patel, N.; Landgraf, R.; Wilson, J. N. *Bioorg. Med. Chem. Lett.* **2012**, *22*, 5532-5535.
5. Dhuguru, J.; Liu, W.; Gonzalez, W. G.; Babinchak, W. M.; Miksovska, J.; Landgraf, R.; Wilson, J. N. *J. Org. Chem.* **2014**, *79*, 4940-4947.
6. Lee, H.; Liu, W.; Brown, A. S.; Landgraf, R.; Wilson, J. N. *Anal. Chem.* **2016**, *88*, 11310-11313.
7. Bridges, A. J. *Chem. Rev.* **2001**, *101*, 2541-2571.
8. Rewcastle, R.W.; Denny, W. A.; Bridges, A. J.; Zhou, H.; Cody, D. R.; McMichael, A.; Fry, D.W. *J. Med. Chem.* **1995**, *38*, 3482-3487.
9. Levinson, N. M.; Boxer, S. G. *PLoS One*, **2012**, *7*, e29828.
10. Wilson, J. N.; Liu, W.; Brown, A. S.; Landgraf, R. *Org. Biomol. Chem.* **2015**, *13*, 5006-5011.
11. Trummer, B. J.; Iyer, V.; Balu-Iyer, S. V.; O'Connor, R.; Straubinger, R. M. *J. Pharm. Sci.*, **2012**, *101*, 2763-2776.
12. Wissner, A.; Berger, D. M.; Boschelli, D. H.; Floyd, M. B.; Greenberger, L. M.; Gruber, B. C.; Johnson, B. D.; Mamuya, N.; Nilakantan, R.; Reich, M. F.; Shen, R.; Tsou, H. -R.; Upeslacis, E.; Wang, Y. F.; Biqi Wu, B.; Fei Ye, F.; Zhang, N. *J. Med. Chem.* **2000**, *43*, 3244-3256.
13. Wissner, A.; Mansour, T. S. *Arch. Pharm. Chem. Life Sci.* **2008**, *341*, 465-477.
14. Pannala, M.; Kher, S.; Wilson, N.; Gaudette, J.; Sircar, I.; Zhang, S. -H.; Bakhirev, A.; Yang, G.; Yuen, P.; Gorcsan, F.; Sakurai, N.; Barbosa, M.; Cheng, J. -F. *Bioorg. Med. Chem. Lett.* **2007**, *17*, 5978-5982.

15. Reichardt, C. *Angew. Chem. Int. Ed. Engl.* **1979**, *18*, 98-110.
16. Zhao, C.; An, J.; Zhou, L.; Fei, Q.; Wang, F.; Tan, J.; Shi, B.; Wang, R.; Guo, Z.; Zhu, W. -H. *Chem. Commun.* **2016**, *52*, 2075-2078.
17. Zhang, Y. –M.; Cockerill, S.; Guntrip, S. B.; Rusnak, D.; Smith, K.; Vanderwall, D.; Wood, E.; Lackey, K. *Bioorg. Med. Chem. Lett.*, **2004**, *14*, 111-114.
18. Knight, L. A.; Di Nicolantonio, F.; Whitehouse, P.; Mercer, S.; Sharma, S.; Glaysher, S.; Johnson, P.; Cree, I. A. *BMC Cancer*, **2004**, *4*, 83-90.
19. Jain, A.; Tindell, C. A.; Laux, I.; Hunter, J. B.; Curran, J.; Galkin, A.; Afar, D. E.; Aronson, N.; Shak, S.; Natale, R. B.; Agus, D. B. *Proc. Nat. Acad. Sci. USA*, **2005**, *102*, 11858-11863.
20. Piechocki, M. P.; Yoo, G. H.; Dibbley, S. K.; Lonardo, F. *Cancer Res.* **2007**, *67*, 6825-6843.
21. Hendriks, B. S.; Opresko, L. K.; Wiley, H. S.; Lauffenburger, D. *J. Biol. Chem.* **2003**, *278*, 23343-23351.
22. Hirata, A.; Hosoi, F.; Miyagawa, M.; Ueda, S.-i.; Naito, S.; Fujii, T.; Kuwano, M.; Ono, M. *Cancer Res.* **2005**, *65*, 4253-4260.
23. Paez, J. G.; Jänne, P. A.; Lee, J. C.; Tracy, S.; Greulich, H.; Gabriel, S.; Herman, P.; Kaye, F. J.; Lindeman, N.; Boggon, T. J.; Naoki, K.; Sasaki, H.; Fujii, Y.; Eck, M. J.; Sellers, W. R.; Johnson, B. E.; Meyerson, M. *Science* **2004**, *304*, 1497-1500.
24. Björkelund, H.; Gedda, L.; Barta, P.; Malmqvist, M.; Andersson, K. *PLoS One*, **2011**, *6*, e24793.
25. Björkelund, H.; Gedda, L.; Barta, P.; Malmqvist, M.; Andersson, K. *Mol. Clin. Oncol.* **2013**, *1*, 343-352.
26. Citri, A.; Alroy, I.; Lavi, S.; Rubin, C.; Xu, W.; Grammatikakis, N.; Patterson, C.; Neckers, L.; Fry, D. W.; Yarden, Y. *EMBO J.* **2002**, *21*, 2407-2417.
27. Sánchez-Martín, M.; Pandiella, A. *Int. J. Cancer.* **2012**, *131*, 244-252.
28. Zhang, Y.; Zhang, J.; Liu, C.; Du, S.; Feng, L.; Luan, X.; Shi, Y.; Wang, T.; Wu, Y.; Cheng, W.; Meng, S.; Li, M.; Liu, H. *Cancer Lett.*, **2016**, *382*, 176-185.
29. Citri, A.; Gan, J.; Mosesson, Y.; Vereb, G.; Szollosi, J.; Yarden, Y. *EMBO Rep.*, **2004**, *5*, 1165-1170.
30. Warren, C. M.; Landgraf, R. *Cell. Signal.* **2006**, *18*, 923-933.
31. Bertelsen, V.; Stang, E. *Membranes* **2014**, *4*, 424-446.
32. Sigismund, S.; Confalonieri, S.; Ciliberto, A.; Polo, S.; Scita, G.; Di Fiore, P. P. *Physiol. Rev.* **2012**, *92*, 273-366.
33. Schindelin, J; Arganda-Carreras, I.; Frise, E.; Kaynig, V.; Longair, M.; Pietzsch, T.; Preibisch, S.; Rueden, C.; Saalfeld, S.; Schmid, B.; Tinevez, J. –Y.; White, D. J.; Hartenstein, V.; Eliceiri, K.; Tomancak, P.; Cardona, A. *Nature Meth.* **2012**, *9*, 676.

Supplementary Material

Please see ^{1}H and ^{13}C NMR spectra for **2**-**4**, **CQ**, **CQ1** and **CQ2** as well as atomic coordinates from DFT calculations for **CQ** and **QA** in accompanying file.